

Article

A Comparative Study on Damage Mechanism of Sandwich Structures with Different Core Materials under Lightning Strikes

Jiangyan Yan ¹, Guozheng Wang ² , Qingmin Li ^{1,*}, Li Zhang ², Joseph D. Yan ³, Chun Chen ⁴ and Zhiyang Fang ⁴

¹ State Key Lab of Alternate Electrical Power System with Renewable Energy Sources, North China Electric Power University, Beijing 102206, China; yanjiangyan@ncepu.edu.cn

² School of Electrical Engineering, Shandong University, Jinan 250061, China; guozhengwang@foxmail.com (G.W.); zhlieee@gmail.com (L.Z.)

³ Department of Electrical Engineering and Electronics, The University of Liverpool, Liverpool L69 3GJ, UK; yaneee@liverpool.ac.uk

⁴ Sinoma Wind Power Blade Co., Ltd., Beijing 102100, China; chenchun@sinomablade.com.cn (C.C.); fangzhy@sinomatech.com (Z.F.)

* Correspondence: lqmeee@ncepu.edu.cn; Tel.: +86-10-6177-2040

Received: 30 August 2017; Accepted: 28 September 2017; Published: 13 October 2017

Abstract: Wind turbine blades are easily struck by lightning, a phenomenon that has attracted more and more attention in recent years. On this subject a large current experiment was conducted on three typical blade sandwich structures to simulate the natural lightning-induced arc effects. The resulting damage to different composite materials has been compared: polyvinyl chloride (PVC) and polyethylene terephthalate (PET) suffered pyrolysis and cracks inside, while the damage to balsa wood was fibers breaking off and large delamination between it and the resin layer, and only a little chemical pyrolysis. To analyze the damage mechanism on sandwich structures of different materials, a finite element method (FEM) model to calculate the temperature and pressure distribution was built, taking into consideration heat transfer and flow expansion due to impulse currents. According to the simulation results, PVC had the most severe temperature and pressure distribution, while PET and balsa wood were in the better condition after the experiments. The temperature distribution results explained clearly why balsa wood suffered much less chemical pyrolysis than PVC. Since balsa wood had better thermal stability than PET, the pyrolysis area of PET was obviously larger than that of balsa wood too. Increasing the volume fraction of solid components of porous materials can efficiently decrease the heat transfer velocity in porous materials. Permeability didn't influence that much. The findings provide support for optimum material selection and design in blade manufacturing.

Keywords: wind turbine blade; lightning strikes; materials damage; finite element method (FEM); temperature distribution; airflow pressure

1. Introduction

Wind energy exploitation is seeing rapid development due to its renewable and environmentally-friendly characteristics. However, lightning strikes on wind turbines, especially on the blades, have become an urgent problem as wind turbines have become higher [1–4]. Blade repair is very costly because of the required disassembly and transport, and it influences the continuity of the power supply too.

Wind turbine blades are composite structures made of laminates with sandwich configurations made from individual sub-components joined together with adhesives. A real blade is shown in Figure 1a, and the cross-section of the blade is shown in Figure 1b. It can be seen in Figure 1b that the blade

consists of two coverings (upper and lower covering stuck together) and two webs inside to hold up the blade structure. The green parts are the main beam and the back trailing edge made of very thick glass fiber to guarantee blade strength. The green-yellow parts are porous sandwich structures, with polyvinyl chloride (PVC), polyethylene terephthalate (PET) or balsa wood fused together to reduce the weight of the whole blade, and usually two layers of glass fiber outside. There are two webs inside the chamber to hold up the blade too.

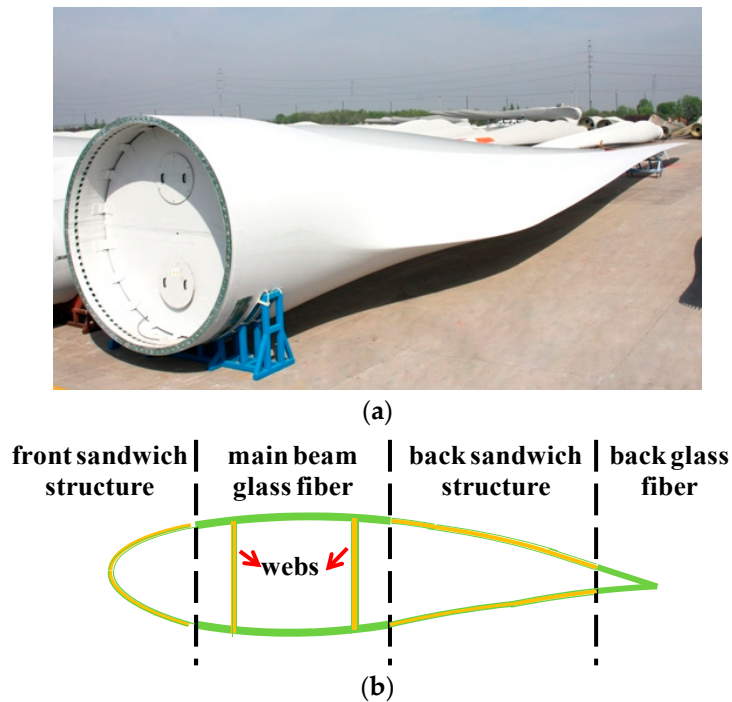


Figure 1. Blade structure: (a) real blade; (b) cross-section of blade.

When receptors on a blade fail to intercept a lightning strike downward leader, the blade materials could suffer breakdown as the lightning-induced arc goes through the sandwich structure. Then blade materials would be burnt up, leading to the layers pulling apart and even the whole blade breaking off [5–9]. A lot of research on lightning strike position has been done by experimental and numerical methods recently [10,11]. In [12], high voltage experiments were conducted to study possible breakdown positions, and the results showed that the breakdown points were mostly located in the sandwich areas, so the performance of the sandwich structure under the thermal effect of lightning-induced arcs is of great importance from a blade material selection viewpoint.

Large current experiments were introduced and laid down in the IEC 61400-24: 2010 standard to verify the performance of metal receptors under the thermal impact of natural lightning [13], and current experiments used to study the damage characteristics of wind turbine blades were also reported in [14–19]. Especially, in [20], the performance of PVC and balsa wood under lightning currents was studied by large current experiments, and their damage mechanisms were explained via molecular dynamics simulation from the angle of chemical pyrolysis. However, studies on the damage characteristics of whole sandwich structures haven't been reported yet. Actually, material damage under large current conditions is mainly attributed to the thermal impact and airflow pressure inside the porous materials (PVC, PET and balsa wood), so it is essential to study the temperature and pressure distribution inside the sandwich structure. Numerical calculation is an effective way to study the instantaneous impact which is really difficult using experimental methods. finite element method (FEM) simulation of thermal and electrical fields under lightning strikes has been proposed by different

researchers [21–23], but heat transfer and air flow pressure inside porous materials need to be included too so as to study the whole damage process of sandwich structures.

This paper deals with the damage characteristics of sandwich structures with different core materials using large current experiments, and a FEM model was built to calculate the temperature and pressure distribution. Based on the above results, the damage characteristics for different materials were studied experimentally and comparatively. The findings provide important advice for blade material selection during the turbine blade manufacturing process.

2. Large Current Experiments

2.1. Experimental Methods

In the experiments the blade was simplified into an F-structure (a simplified model of the blade covering and two webs to hold up the covering) as shown in Figure 2, and the covering was made of resin and porous materials (PVC, PET and balsa wood) by a vacuum casting method. The overall size of all samples is 80 cm × 99 cm, and the heights of each part are 10, 42, 35 and 12 cm, respectively (up to down). In the sandwich structure, 0.6 cm thick PVC, PET and balsa wood were parceled in the middle, with two layers of 0.9 mm thick glass fiber reinforced epoxy resin wrapped outside. The material parameters are listed in Table 1. For the porous materials (PVC, PET and balsa wood), the thermal conductivity, specific heat at constant pressure and density in the table show volume averaging values considering the air component. Balsa wood has different thermal conductivities in different orientations because of its anisotropic characteristics (significantly larger along the fiber direction), so the values in Table 1 are the extreme values. Holes were drilled in the samples and a 0.01 cm diameter nickel chrome wire was passed through each hole to conduct a large current in the different positions shown as red points in Figure 2d (bigger size and number mean larger current values). The pulse current generator is shown in Figure 3. The capacitor voltage (u) was charged to 7.5, 15 and 30 kV, respectively, to generate large pulse currents with parameters (intensity and duration) of 6.28 kA (peak value of current), 7.7 (time to peak)/18.1 (half peak time) μ s, 12.56 kA, 6.7/15.5 μ s and 21 kA, 5.1/13.1 μ s. According to $W = 1/2 Cu^2$ ($C = 15.96 \mu$ F, is the capacitor charging value), the current energy can be obtained as 798, 1795.5 and 3192 J. Then the damage characteristics were comparatively studied.

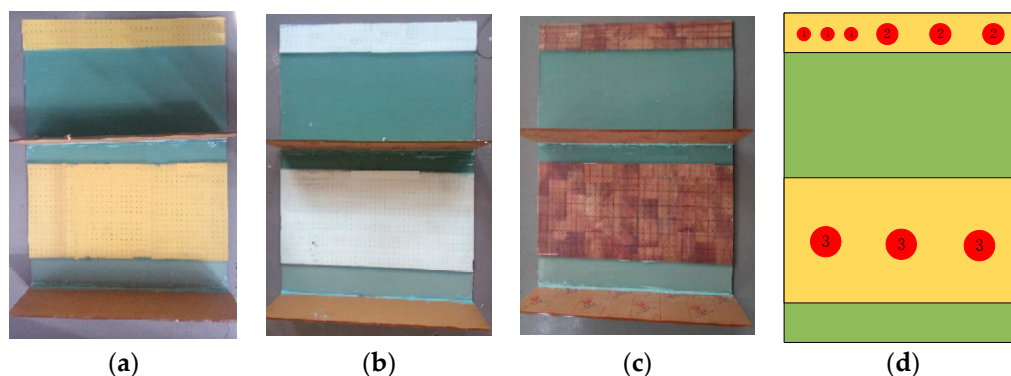
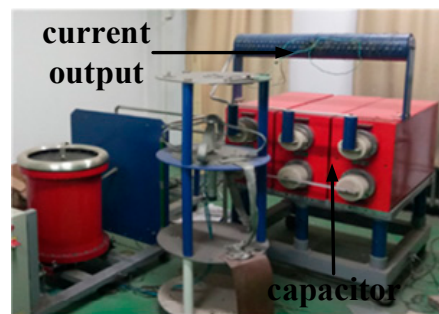


Figure 2. Experimental samples: (a) PVC; (b) PET; (c) balsa wood; (d) nickel chrome wire position.

Table 1. Material parameters.

Materials	Type	Thermal Conductivity, k, W/(m·K)	Specific Heat, C, J/(kg·K)	Density, ρ , kg/m ³	Glass Transition Degree, Tg, K	Solid Fraction θ (%)
Epoxy resin	SWANCOR 2511-1A/1BS	0.4749	989.58	1200	363	100
PVC	3A C70.55	0.0331	1003	66	355	8
PET	3A T92.100	0.0399	1166	98	340	13
Balsa wood	3A SB100	0.0803/0.0661	1047	92	543	11

**Figure 3.** Pulse current generator.

2.2. Results and Discussion

All the samples were damaged to, different degrees as shown in Figure 4. To see the inside condition clearly, damaged parts were cut down and pulled apart as shown in Figure 5. PVC and PET sandwich samples displayed different damage types with respect to balsa wood. They were burnt, with a black coloration near the metal wire, and a large lighter colored area as shown in Figure 4 which indicated delamination between resin and porous materials because of airflow expansion damage. Balsa wood was not burnt severely because of its higher pyrolysis temperature, its fibers broke off near the metal wire and large scale delamination between the interface of the balsa wood and resin can be seen in Figure 4c. The sizes of the (approximately circular) chemical damage (cd, chemical pyrolysis of core materials which appears as black color in Figures 4 and 5) and mechanical damage (md, material disappearance in light colored area, shown in Figure 5 and the delamination area between the resin and core materials shown in Figure 4) areas were measured in all cases as shown in Table 2. The data reflects that PVC and PET had similar chemical damage radii, but the cd of balsa was very small. This is because balsa wood has higher thermal stability (glass transition temperature) than PVC and PET. In the aspect of md, balsa wood had the biggest delamination size between the resin and balsa wood. Mechanical damage of PVC, PET and balsa wood under pulsed currents is mainly caused by the high temperature and airflow expansion inside, which are hard to measure in experiments, thus a FEM simulation study on the damage characteristics of the sandwich structures was done to quantitatively calculate the temperature and pressure distribution.

Table 2. Damage radius (cm).

Current Peak Value (kA)	6.28		12.56		21	
	cd	md	cd	md	cd	md
PVC	0.11	0.50	0.35	3.5	1.7	6.10
PET	0.07	0.45	0.21	3.0	1.5	5.50
Balsa wood	0.01	0.75	0.09	4.1	0.39	7.50

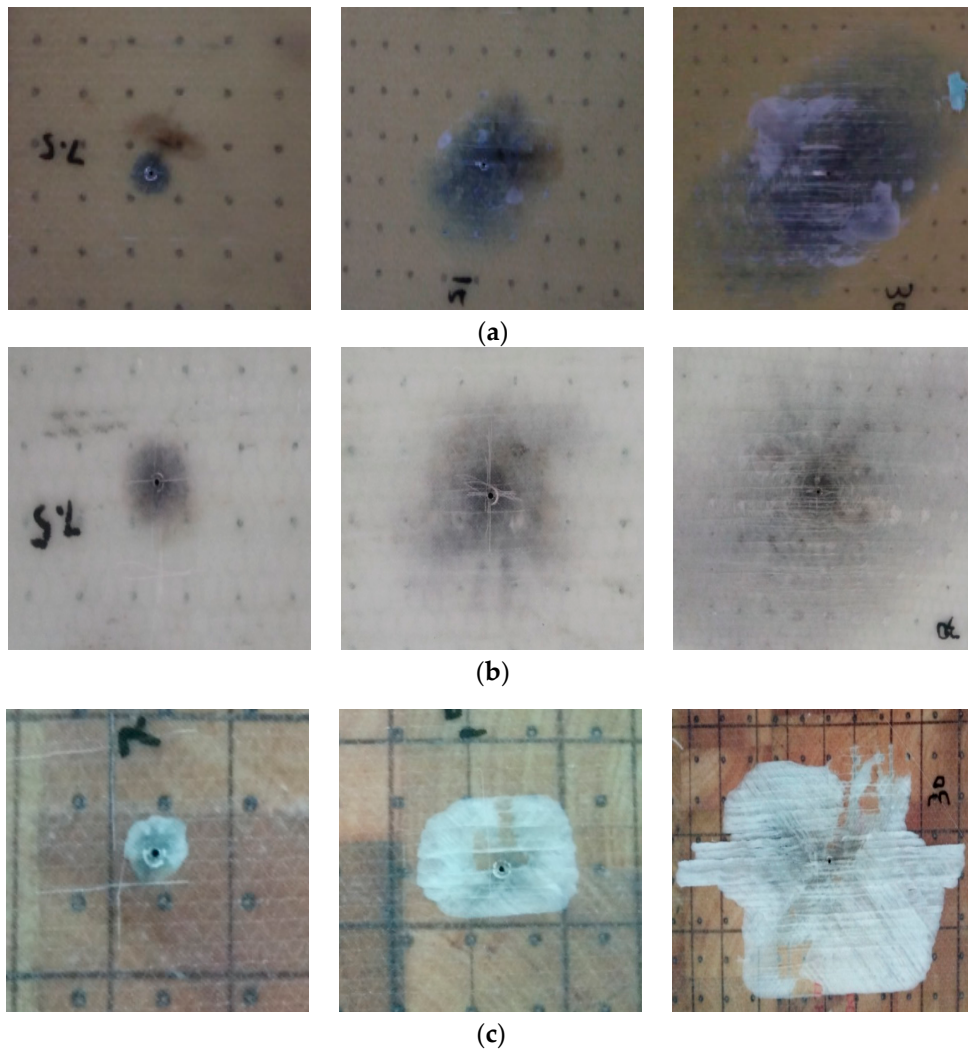


Figure 4. Damage morphology of samples: (a) PVC; (b) PET; (c) balsa wood.

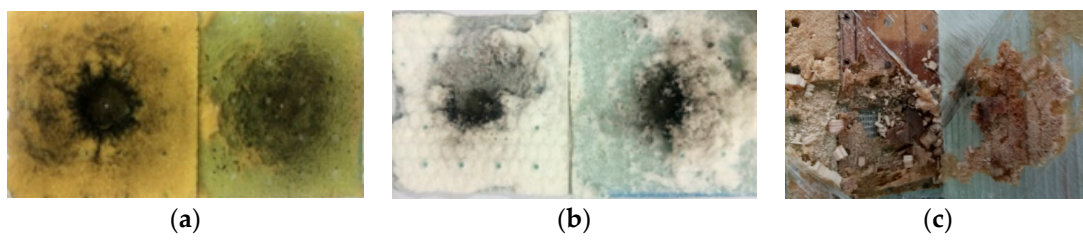


Figure 5. Inside damage of samples: (a) PVC; (b) PET; (c) balsa wood.

3. Numerical Study on the Temperature and Pressure Distribution

A FEM model in COMSOL 5.2a was built to calculate temperature and pressure distribution in the sandwich structures [24].

3.1. Simulation Model

3.1.1. Geometry Model

As can be seen from the experimental results, the damage is distributed in a circular area, so experimental samples to be simulated by the FEM model were simplified into a 2-D axisymmetric model with a proper radius, as shown in Figure 6.

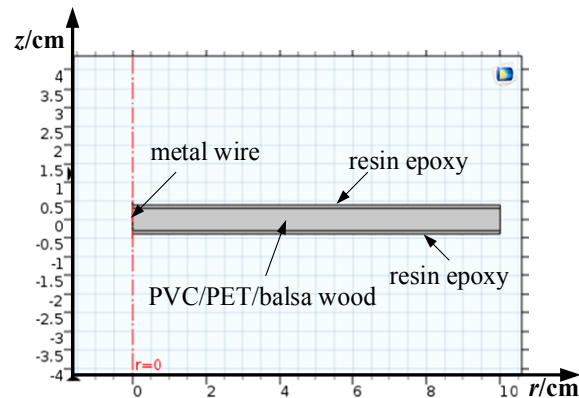


Figure 6. 2-D axisymmetric model for the FEM simulations.

3.1.2. Large Current Source

The heat source was given as a large current in the FEM model. The current conservation Equation (1) was applied to calculate the current density, by which resistive heat can be obtained as heat source by Equation (2). Scalar electric potential is provided as the dependent variable as shown in (3):

$$\mathbf{J} = (\sigma + \varepsilon_0 \varepsilon_r \frac{\partial}{\partial t}) \mathbf{E} \quad (1)$$

$$Q = \frac{J^2}{\sigma} \quad (2)$$

$$\mathbf{E} = -\nabla V \quad (3)$$

where \mathbf{J} , current density; σ , conductivity of nickel-chrome wire; ε_0 , permittivity of vacuum; ε_r , relative permittivity of nickel-chrome wire; \mathbf{E} , electrical field intensity; V , electric potential which was applied on the top of nickel-chrome wire, and simplified to be a linear piecewise function, (see Equation (4)) where $A = 6.28 \text{ kA}$, 12.56 kA and 21 kA , are peak values of pulse current and $R = 0.78 \Omega$ is the resistance of nickel chrome wire:

$$V = \begin{cases} RA \times 10^5 t & t < 10^{-6} \\ R(-A \times 10^5 t + 2A) & 10^{-5} \text{ s} < t < 20^{-6} \text{ s} \end{cases} \quad (4)$$

3.1.3. Heat Transfer in Solids, Porous Materials

The first law of thermodynamics, commonly referred to as the principle of conservation of energy was used to calculate the heat transfer in different areas. For the nickel-chrome wire and resin parts, the equation for heat transfer in solids was applied as Equation (5):

$$\rho C \frac{\partial T}{\partial t} - \nabla \cdot (k \nabla T) = Q \quad (5)$$

where T , temperature; t , time; ρ , density; C , heat capacity; k , thermal conductivity; Q , heat source.

The first term on the left is the energy increase of the whole system, and the second term is the heat flux by conduction from neighboring elements because of the temperature gradient. PVC, PET and balsa wood are porous materials, and they have a similar conservation of energy expression as shown in Equation (6). Comparing Equations (6) and (5) for a solid material, $\rho_g C_g \mathbf{u} \cdot \nabla T$ was added to describe the heat flux by gas convection from neighboring elements. Since there is gas fraction in the porous materials, heat transfer by gas convection should be included too.

Heat capacity and thermal conductivity of porous materials were calculated by volume averaging of gas and solid components, as shown in Equations (7) and (8):

$$\rho C \frac{\partial T}{\partial t} + \rho_g C_g \mathbf{u} \cdot \nabla T - \nabla \cdot (k \nabla T) = Q \quad (6)$$

$$\rho C = \theta \rho_g C_g + (1 - \theta) \rho_s C_s \quad (7)$$

$$k = \theta k_g + (1 - \theta) k_s \quad (8)$$

where \mathbf{u} , velocity field; ρ_s , solid density; C_s , solid heat capacity; k_s , solid thermal conductivity; ρ_g , air density, it changes with temperature T and pressure P , that is $\rho_g = PM_g / (RT)$. $M_g = 28.97$ g/mol, is the air molar mass and $R = 8.314$ J/(mol·K), is the gas constant; C_g , gas heat capacity; k_g , gas thermal conductivity; ρ , C and k are density of porous matrix; θ is porosity.

To simulate practical conditions, all outer boundaries were set as Equation (9) considering the convection process between samples and the external atmosphere:

$$-\mathbf{n} \cdot \mathbf{q} = h(T_{ext} - T) \quad (9)$$

where \mathbf{n} is the normal vector; \mathbf{q} is the heat flux on the boundaries; $h = 15$ W/(m²·K) is the heat transfer coefficient on the materials' surface; T_{ext} is the atmosphere temperature.

3.1.4. Fluid Dynamics in Porous Materials

Brinkman equations was adopted to calculate the fluid dynamics in porous materials. The flow in porous media is governed by a combination of the continuity Equation (10) and the momentum conservation Equation (11), which together form the Brinkman equations. Pressure P and velocity vector \mathbf{u} are independent variables:

$$\frac{\partial}{\partial t}(\theta \rho_g) + \nabla \cdot (\rho_g \mathbf{u}) = Q_{br} \quad (10)$$

$$\frac{\rho_g}{\varepsilon} \left(\frac{\partial \mathbf{u}}{\partial t} + (\mathbf{u} \cdot \nabla) \frac{\mathbf{u}}{\varepsilon} \right) = -\nabla P + \nabla \cdot \left\{ \frac{1}{\varepsilon} [\mu (\nabla \mathbf{u} + (\nabla \mathbf{u})^T) - \frac{2}{3} \mu (\nabla \cdot \mathbf{u}) \mathbf{I}] \right\} - (\kappa^{-1} \mu + \frac{Q_{br}}{\varepsilon^2}) \mathbf{u} + \mathbf{F} \quad (11)$$

where μ , dynamic viscosity of air in porous materials; \mathbf{u} , velocity vector; P , pressure; $\kappa = 1 \times 10^{-13}$ m², permeability tensor of the porous medium; $Q_{br} = 0$, mass source or mass sink; \mathbf{F} , force term, influence of gravity and other volume forces, and it was neglected in this model. To simulate real conditions, the right boundary was set as the outlet boundary, and $\mathbf{u} = 0$ for other boundaries to baffle the expansion flow.

3.1.5. Multi-Physics Coupling

The above discussed calculation procedure involving a coupled threefold physics, as shown in Figure 7, allowed us to obtain the temperature T and pressure P . A damage process lasting 1000 μ s was simulated.

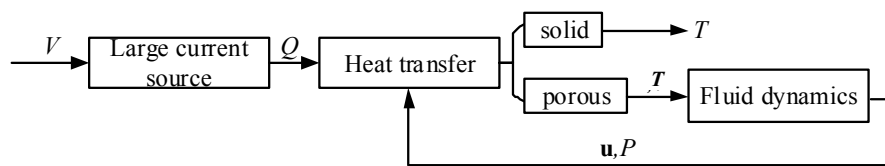


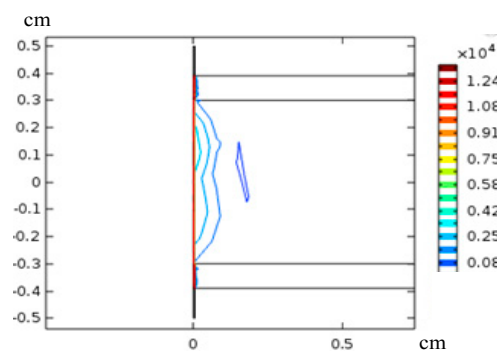
Figure 7. Multi-physics coupling.

3.2. Simulation Results

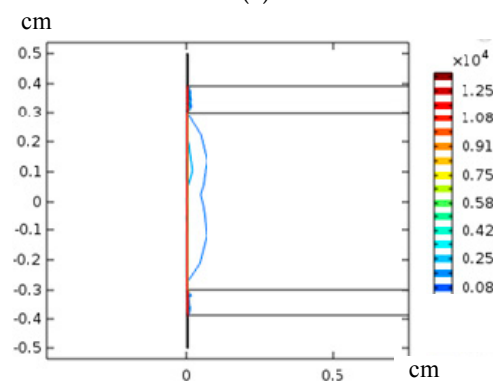
3.2.1. Temperature Distribution

Temperature distributions after calculations inside the sandwich materials are shown in Figure 8. It can be seen that heat is transferred much quicker in porous materials than in resin. It is because that airflow convection promotes the heat transfer inside the porous material, especially under the very big fluid velocity resulting from an impulse energy of thousands of degrees. The resin layer conducted heat slowly and most of the heat is released to the atmosphere, so there was no serious damage in this area.

PVC porous material had smallest solid fraction, that is, the highest air fraction, so its high temperature scale was obviously larger than others. Simulation areas with temperatures above the glass transition temperature were considered as chemical damage areas, which turned black in practice. Then the chemical damage radius of different materials was estimated with respect to time as shown in Figure 9. The last data connected by dotted lines is the experimental results in Table 2. It can be seen that the simulation data trend fitted well with the experimental results. The chemical damage radius increased quickly when the current peak value was raised. Balsa wood had smallest chemical damage radius among the three materials because of its highest glass transition temperature. PVC had the largest radius because of its higher temperature distribution.



(a)



(b)

Figure 8. Cont.

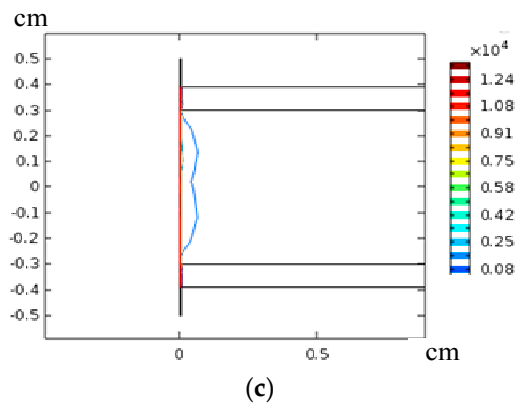


Figure 8. Isothermal curve in sandwich models (peak value of 12.56 kA, 50 μ s): (a) PVC; (b) PET; (c) balsa wood.

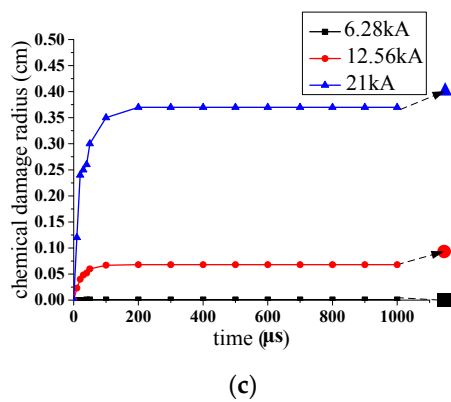
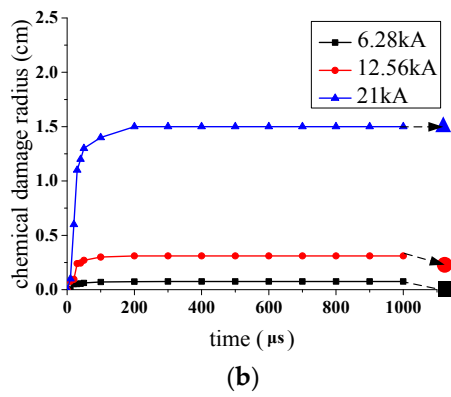
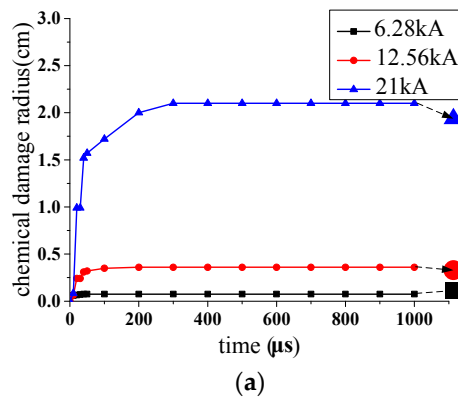


Figure 9. Chemical damage radius of porous materials: (a) PVC; (b) PET; (c) balsa wood.

3.2.2. Pressure Distribution

Porous materials also suffer severe physical damage from inner flow pressure. The pressure distribution at 200 μ s is shown in Figure 10. Consistent with the temperature distribution, PVC is expected to suffer a much more severe fluid impact pressure than PET and balsa wood because of high temperature and large air fraction. The peak value of pressure in different points on the center line in the r-direction is shown in Figure 11. In the case of balsa wood, it performs better inside, but when high pressure occurred at its interface with resin, large delamination happened because of the weak bonding between the wood and the resin.

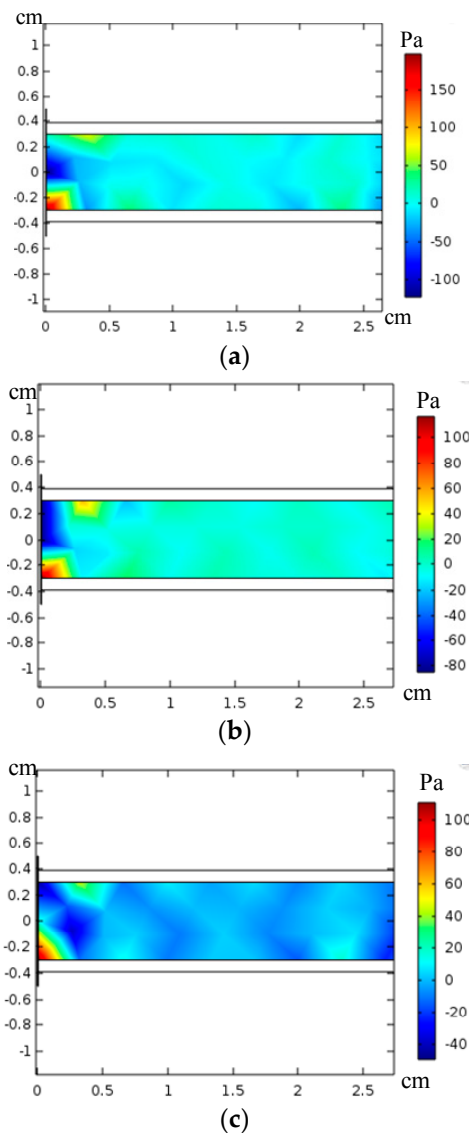


Figure 10. Pressure distribution in porous areas (peak value of 6.28 kA, 200 μ s): (a) PVC; (b) PET; (c) balsa wood.

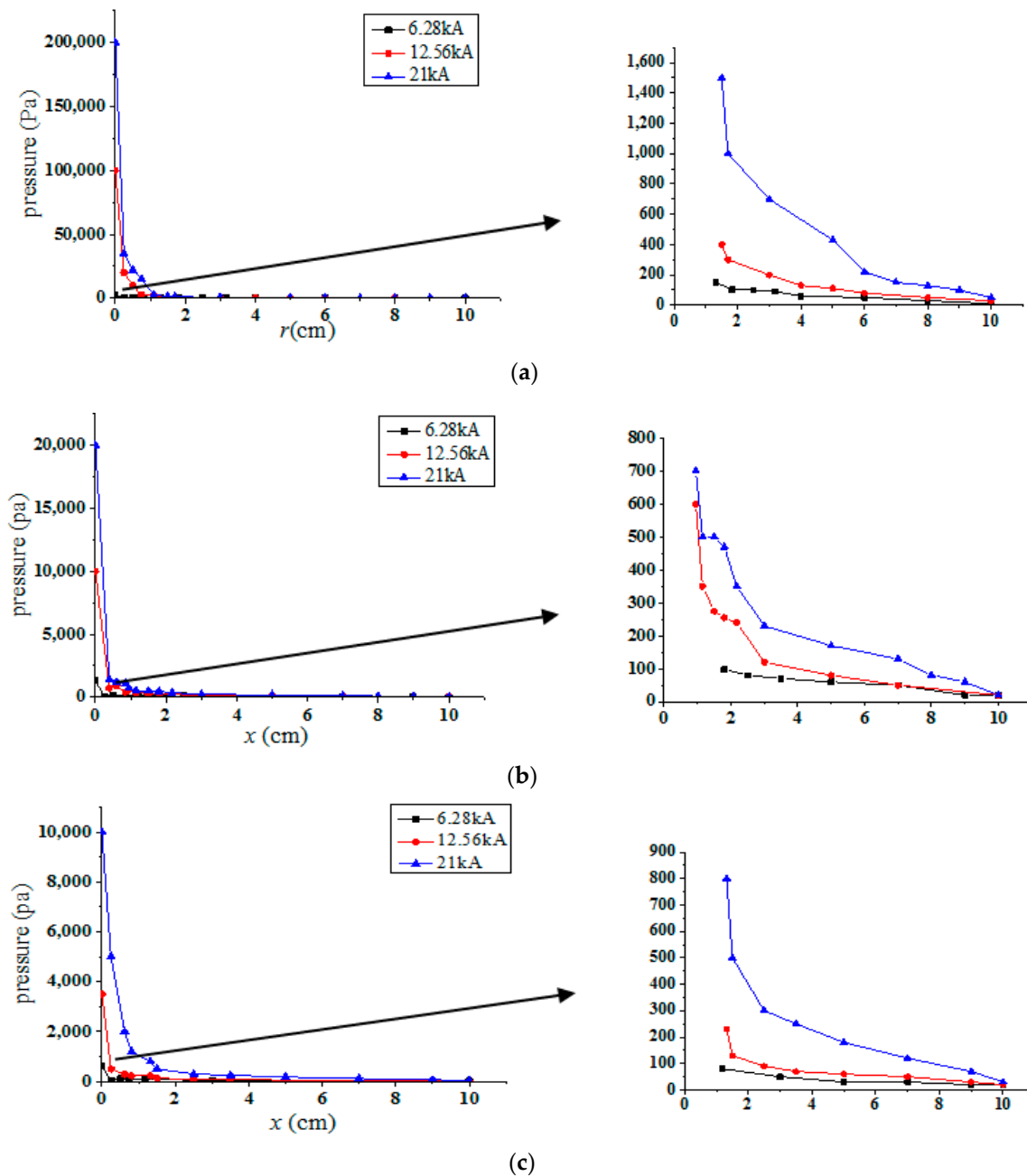


Figure 11. Pressure distribution on center line of porous materials: (a) PVC; (b) PET; (c) balsa wood.

3.2.3. Influence of Porosity, Permeability

Solid materials' volume fraction (θ) and permeability are the main parameters for porous materials in heat transfer and fluid dynamics process. Based on the above model, the roles of porosity and permeability were analyzed which helped materials designing for wind turbine blade. Since permeability hardly influenced the thermal conducting and airflow expansion process because of the very small dynamic viscosity of air (see Equation (11)), only results for different porosities will be presented.

Glass transition scale and area radius where $P > 100$ Pa were set as standards for thermal and fluid dynamics results. θ of real value as shown in Table 1, where two times the real value, three times the real value and five times the real value were used to compare their influence, as shown in Tables 3 and 4. It is indicated that increasing the solid fraction obviously decreases the damage area. This can be explained in the following way: when a large current goes through a porous material, the heat transfers

through three ways: heat conduction by the solid fraction, heat convection by the gas fraction and heat going out by the current channels to the outside environment. Compared to the heat conduction by the solid fraction (PVC, PET and balsa wood are not very good at conducting heat), the heat convection by the gas fraction and heat going out play more important roles in the heat transfer because the airflow has a very large velocity. Heat convection by the gas fraction accelerates heat to be transferred to a larger porous material region to cause more severe damage, so if the gas fraction of a porous material is decreased, that is, the solid fraction is increased, the damaged area can be decreased, and more energy goes out by the current channels to the outside environment.

Table 3. Glass transition scale reduction (%) with θ .

Solid Fraction	1 Time	2 Times	3 Times	5 Times
PVC	0	22.5	68.7	72.6
PET	0	17.7	70	73.3
Balsa wood	0	30.7	49.3	86.7

Table 4. Pressure (>100 Pa) area radius reduction (%) with porosities.

Solid Fraction	1 Time	2 Times	3 Times	5 Times
PVC	0	2.6	5.1	23.1
PET	0	3.6	22.1	26.3
Balsa wood	0	3.2	20.6	25.9

4. Conclusions

Large current experiments to compare the damage characteristics of turbine blade sandwich structures with different core materials were conducted in this experimental study, and a FEM simulation was used to reveal the damage mechanism. Combining the experiments and simulation results, the following can be concluded:

1. PVC, PET and balsa wood all underwent severe damage under a large current, but their damage types were different: PVC and PET suffered serious pyrolysis and cracks inside, while the damage of the balsa wood sample involved fibers breaking off and large delamination at its interface with the resin layer. Balsa wood was burnt only in a little under the experimental current used.
2. Porous materials transferred heat much faster than the resin layer, because the fast air-flow convection under the thermal impact from lightning strongly promoted heat transfer in the porous material layer.
3. PVC sample had highest average value of temperature and pressure because of its highest air fraction and airflow convection, so it suffered the biggest mechanical damage and chemical damage; and balsa wood suffered relatively less chemical damage because of its higher glass transition temperature. Balsa wood is very soft, which makes it good at reducing the expansion pressure inside, while bad bonding between it and resin layer resulted in large delamination at the interface with the resin. However, when the energy of the lightning current is extremely large, balsa wood usually catches fire more likely than PVC and PET because of its own characteristics, and under the worst conditions, this fire can last for a long time and cause a serious fire hazard.
4. If the gas fraction of the porous materials is decreased, that is, the solid fraction is increased, the heat transfer by gas convection in the porous materials can be decreased. Then the damaged area can be reduced and more energy goes out by the current channels to the outside environment in practice. This is a good way to reduce the scale of damage to porous materials under lightning strike conditions.

Acknowledgments: This work was supported by the National Natural Science Foundation of China (grant numbers 51420105011, 51677110).

Author Contributions: Jiangyan Yan conceived and designed the experiments; Qingmin Li, Li Zhang and Joseph D. Yan gave important advice on the experiments; Chun Chen and Zhiyang Fang contributed experimental materials; Jiangyan Yan and Guozheng Wang performed the experiments; Jiangyan Yan performed the simulation, analyzed the data and finally wrote the paper.

Conflicts of Interest: The authors declare no conflicts of interest.

References

1. Candela, G.A.; Find, M.S.; Nissim, M. Lightning damage to wind turbine blades from wind farms in the U.S. *IEEE Trans. Power Deliv.* **2016**, *31*, 1043–1049. [[CrossRef](#)]
2. Napolitano, F.; Paolone, M.; Borghetti, A. Models of wind-turbine main-shaft bearings for the development of specific lightning protection systems. *IEEE Trans. Electromagn. Compat.* **2011**, *53*, 99–107. [[CrossRef](#)]
3. Rodrigues, B.; Mendes, F.; Catalão, S. Protection of wind energy systems against the indirect effects of lightning. *Renew. Energy* **2011**, *36*, 2888–2996. [[CrossRef](#)]
4. Li, X.; Wang, J.; Wang, Y. Lightning transient characteristics of cable power collection system in wind power plants. *IET Renew. Power Gener.* **2015**, *9*, 1025–1032. [[CrossRef](#)]
5. Candela, G.A. Lightning Protection of Flap System for Wind Turbine Blades. Ph.D. Thesis, Technical University of Denmark, Lyngby, Denmark, 2014.
6. Yokoyama, S.; Yasuda, Y.; Minowa, M.; Sekioka, S. Clarification of the mechanism of wind turbine blade damage taking lightning characteristics into consideration and relevant research project. In Proceedings of the International Conference on Lightning Protection (ICLP), Vienna, Austria, 2–7 September 2012.
7. Yasuda, Y.; Yokoyama, S.; Ideno, M. Verification of lightning damage classification to wind turbine blades. In Proceedings of the International Conference on Lightning Protection (ICLP), Vienna, Austria, 2–7 September 2012.
8. Arinaga, S.; Tsutsumi, K. Experimental study on lightning protection methods for wind turbine blades. In Proceedings of the International Conference on Lightning Protection, Kanazawa, Japan, 18–22 September 2006.
9. Yokoyama, S. Lightning protection of wind turbine blades. *Electr. Power Syst. Res.* **2013**, *94*, 3–9. [[CrossRef](#)]
10. Zhou, M.; Wang, J.; Fan, Y. Experimental study of lightning strike attachment characteristics on wind turbine generators. In Proceedings of the International Conference on Lightning Protection (ICLP), Estoril, Portugal, 25–30 September 2017.
11. Long, M. On the Attachment of Lightning Flashes to Wind Turbines. Ph.D. Thesis, KTH Royal Institute of Technology, Stockholm, Sweden, 2016.
12. Yan, J.; Li, Q.; Guo, Z. Puncture position on wind turbine blades and arc path evolution under lightning strikes. *Mater. Des.* **2017**, *122*, 197–205. [[CrossRef](#)]
13. International Electrotechnical Commission. *IEC 61400-24: 2010: Wind Turbines—Part 24: Lightning Protection*; IEC: Geneva, Switzerland, 2010.
14. Rachidi, F. A Review of current issues in lightning protection of new generation wind-turbine blades. *IEEE Trans. Ind. Electron.* **2008**, *55*, 2489–2496. [[CrossRef](#)]
15. Radicevi, M.; Savic, S.; Madsen, F.; Badea, I. Impact of wind turbine blade rotation on the lightning strike incidence—A theoretical and experimental study using a reduced-size model. *Energy* **2012**, *25*, 644–654. [[CrossRef](#)]
16. Inoue, K.; Korematsu, Y.; Nakamura, N. Study on damage-mechanism of wind turbine blades by lightning strike. In Proceedings of the International Conference on Lightning Protection, Kanazawa, Japan, 18–22 September 2006.
17. Goda, Y.; Tanaka, S.; Ohtaka, T. Arc Tests of wind turbine blades simulating high energy lightning strike. In Proceedings of the International Conference on Lightning Protection, Uppsala, Sweden, 23–26 June 2008.
18. Ogasawara, T.; Hirano, Y.; Yoshimura, A. Coupled Thermal–Electrical analysis for carbon fiber epoxy composites exposed. *Compos. Part A* **2010**, *41*, 973–981. [[CrossRef](#)]
19. Feraboli, P.; Miller, M. Damage resistance and tolerance of carbon/epoxy composite coupons subjected to simulated lightning strike. *Compos. Part A Appl. Sci. Manuf.* **2009**, *40*, 954–967. [[CrossRef](#)]

20. Yan, J.; Li, Q.; Guo, Z. Damage mechanism of PVC and balsa wood used in wind turbine blade under thermal effect of lightning strikes. In Proceedings of the International Conference on Lightning Protection (ICLP), Estoril, Portugal, 25–30 September 2016.
21. Wang, Y.; Zhupanska, I. Lightning strike thermal damage model for glass fiber reinforced polymer matrix composites and its application to wind turbine blades. *Compos. Struct.* **2015**, *132*, 1182–1191. [[CrossRef](#)]
22. Ding, N.; Zhao, B.; Liu, Z. Simulation of ablation damage of composite laminates subjected to lightning strikes. *Acta Aeronaut. Astronaut. Sin.* **2013**, *34*, 301–308. (In Chinese)
23. Ding, N.; Zhao, B. Analysis of damage influence factors on ablation damage of composite laminates subjected to lightning strikes. *Trans. Mater. Heat Treat.* **2014**, *35*, 186–192. (In Chinese)
24. Yu, C. *Numerical Analysis of Heat and Mass Transfer for Porous Materials*; Tsinghua University Press: Beijing, China, 2011.



© 2017 by the authors. Licensee MDPI, Basel, Switzerland. This article is an open access article distributed under the terms and conditions of the Creative Commons Attribution (CC BY) license (<http://creativecommons.org/licenses/by/4.0/>).